

# Characterization of phase development in commercial Al-Zn-Mg(-Mn,Fe) alloy with and without Sc,Zr-addition

M. Vlach\*, V. Kodetová, B. Smola, J. Čížek, T. Kekule, M. Cieslar, H. Kudrnová, L. Bajtošová, M. Leibner, I. Procházka

Charles University, Faculty of Mathematics and Physics, Ke Karlovu 3, 121 16 Prague, Czech Republic

Received 23 March 2018, received in revised form 23 July 2018, accepted 20 September 2018

## Abstract

Precipitation reactions of the Al-Zn-Mg(-Mn,Fe)-based alloys with/without Sc,Zr-addition were studied by microhardness and resistivity measurements, and differential scanning calorimetry. Microstructure observation proved the Zn,Mg-containing eutectic phase at grain boundaries. Positron spectroscopy confirmed the presence of Guinier-Preston (GP) zones in the initial state. The changes in resistivity and microhardness curves as well as in heat flow are mainly caused by the formation and/or dissolution of the Guinier-Preston zones and precipitation of the particles from the Al-Zn-Mg system. Formation of the Mn,Fe-containing particles as well as of the  $\eta$ - and  $T$ -phase does not influence hardening significantly. The hardening effect above  $\sim 300^\circ\text{C}$  reflects the Sc,Zr-addition. Heat treatment at  $300^\circ\text{C}$  for 60 min and  $460^\circ\text{C}$  for 45 min is insufficient for homogenization of the alloys. The apparent activation energy values were calculated: dissolution of the GP zones ( $\sim 106 \text{ kJ mol}^{-1}$ ), formation of the metastable  $\eta'$ -phase ( $\sim 111 \text{ kJ mol}^{-1}$ ), formation of the stable  $\eta$ -phase ( $\sim 126 \text{ kJ mol}^{-1}$ ) and formation of the  $T$ -phase ( $\sim 144 \text{ kJ mol}^{-1}$ ).

Key words: AA7xxx alloys, early precipitation stages, electrical resistivity, GP zones,  $\text{Al}_3(\text{Sc,Zr})$  particles, activation energy

## 1. Introduction

The commercial Al-Zn-Mg-based alloys (AA7xxx series) have a variety of applications in automotive and aircraft industries due to their high age-hardening response and low density [1–3]. They exhibit reasonable solid solution hardening, but mechanical properties of these alloys logically depend on chemical composition, mainly on Zn and Mg content and on the heat treatment of the studied alloys [2, 4–7]. Although controversies and ambiguities exist about the structures and the species of the hardening precipitates, the precipitation sequence in the alloys has thus far been understood, in terms of precipitation and dissolution of the phases the commonly isothermal sequence is used as (e.g. [2–8]): supersaturated solid solution  $\rightarrow$  Guinier-Preston (GP) zones  $\rightarrow$  semicoherent  $\eta'$ -phase  $\rightarrow$  incoherent  $\eta$ -phase ( $\text{MgZn}_2$ ). Instead of stable  $\eta$ -phase, the formation of the GP zones and  $\eta'$ -phase are proved to be responsible for the peak

strength of the alloys. However, the formation of the GP zones and  $\eta'$ -phase precipitates depends on the alloy composition, artificial ageing temperature, ageing time, heat treatment, etc. [5–8]. The decomposition sequence should also contain metastable semicoherent  $T'$ -phase ( $\text{Al}_2\text{Zn}_3\text{Mg}_3$  – hexagonal structure) and equilibrium  $T$ -phase ( $\text{Al}_2\text{Zn}_3\text{Mg}_3$  – cubic structure) [7–10].

An addition of Sc ( $\sim 0.15 \text{ at.}\%$ ) and Zr ( $\sim 0.1 \text{ at.}\%$ ) to Al-based alloys is made to refine the cast grain structure, to increase recrystallization temperature and to improve mechanical properties [1, 11]. A large improvement of Al due to Sc,Zr-addition has been frequently reported to be the formation of nanoscale, coherent  $\text{Al}_3(\text{Sc,Zr})$ -phase precipitates ( $\text{L1}_2$  structure) [11–13]. It predetermines the Al-Sc-Zr-based alloys for high-temperature automotive and aerospace applications [11]. Consequently, there is an interest in the further improvement of the properties of the Al-Zn-Mg-based alloys containing a level of Sc

\*Corresponding author: tel.: +420221911659; fax: +420221911618, e-mail address: [martin.vlach@mff.cuni.cz](mailto:martin.vlach@mff.cuni.cz)

and Zr and studying their role in microstructure and mechanical properties of the alloys [1]. Even though the AA7xxx series alloys are some of the most extensively used Al-based alloys, relatively few studies (e.g., [14–17]) have investigated the precipitation processes, mechanical and thermal properties of the Al-Zn-Mg-based alloys with Sc and Zr addition. Tailoring material to required properties is very difficult without the detailed knowledge of precipitation processes and the role of Sc and Zr in microstructure development.

The aim of the present work was to study the phase transformations in Al-Zn-Mg(-Mn,Fe) alloys with and without Sc and Zr content in the as-cast, heat-treated, and natural-aged states and the investigation of the microstructure changes during non-isothermal annealing.

## 2. Materials and methods

The Al-5.28at.%Zn-3.47at.%Mg-0.07at.%Mn,Fe (AlZnMg) and Al-5.26at.%Zn-3.54at.%Mg-0.12at.%Mn,Fe-0.14at.%Sc-0.08at.%Zr (AlZnMgScZr) alloys were studied. Heat treatment of the mould-cast state (MC) of the alloys was performed at 300 °C for 60 min and subsequently at 460 °C for 45 min in Ar protective atmosphere or at 460 °C for 45 min only. The annealing was finished by water quenching. The high temperature treated alloy at 460 °C for 45 min is labelled as the heat-treated (HT) one in the text. Two-step high-temperature treatments (at 300 °C for 60 min and subsequently at 460 °C for 45 min) are labelled IN+HT state. The materials were kept in liquid nitrogen at 78 K after quenching until measurements, or other annealing started to avoid possible natural ageing (NA).

The relative electrical resistivity changes  $\Delta\rho/\rho_0$  (RESI) were determined at 78 K within an accuracy of  $10^{-4}$  using the DC four-point method. The influence of parasitic thermo-electromotive force was suppressed by current reversal. Vickers microhardness (HV) testing was performed in Wolpert Wilson Micro Vickers 401MVD at  $\sim 10^\circ\text{C}$ . The measurement of the hardness values started no longer than 60 s after the quenching. Isochronal annealing (effective speed – 1 K min $^{-1}$ ) was carried out in a silicon oil bath (up to 240 °C) or in a furnace with the protective atmosphere (above 240 °C) and each annealing step was finished by quenching into liquid nitrogen or water, respectively. Between measurements, the samples were kept at 78 K to preserve the developed microstructure during the annealing.

The thermal behaviour of the alloys was studied using differential scanning calorimetry (DSC) performed in Netzsch DSC 200 F3 Maia apparatus at heating rates of 1, 2, 5, 10 and 30 K min $^{-1}$  up to 450 °C and at heating rate 20 K min $^{-1}$  up to 500 °C. A specimen of mass between 10–20 mg was placed in Al<sub>2</sub>O<sub>3</sub> crucibles in a dynamic nitrogen atmosphere (40 ml min $^{-1}$ ).

Positron annihilation spectroscopy (PAS) was employed for measurement of positron lifetime (LT) of the MC state of the AlZnMg alloy. The measurements were performed using <sup>22</sup>Na positron source sealed in titanium foil. Detailed information about LT measurements is described in [18].

The measurements mentioned above were compared to microstructure development observed by transmission electron microscopy (TEM) and scanning electron microscopy (SEM). TEM and SEM observations were carried out in JEM 2000FX and MIRA I Schottky FE-SEM microscopes, respectively. The analysis of precipitated phases was complemented by energy-dispersive spectroscopy (EDS) performed by X-ray BRUKER microanalyser. The specimens for TEM and SEM were annealed by the same procedure as those for the electrical resistivity and microhardness measurements. A foil for TEM observations was prepared immediately after heat treatment of the alloy to minimize its natural ageing. The preparation of foil took approximately 40 min.

## 3. Results and discussion

### 3.1. Phase development in the MC alloys during isochronal annealing

The response of the relative resistivity changes  $\Delta\rho/\rho_0$  and microhardness HV1 to step-by-step isochronal annealing in the MC alloys is shown in Fig. 1a. The electrical resistivity curves show a significant decrease of the  $\Delta\rho/\rho_0$  in three stages (I-stage up to  $\sim 150^\circ\text{C}$ , II-stage between 150 and 240 °C, III-stage between 240 and 300 °C) to a minimum. Then the electrical resistivity increases (IV-stage). The initial microhardness HV values of the AlZnMg(ScZr) alloys are comparable in both studied MC alloys, HV  $\approx 126$  for the AlZnMg alloy and HV  $\approx 132$  for the AlZnMgScZr one. The HV values decrease to a local minimum at  $\sim 120^\circ\text{C}$ . The temperature range of the hardening peak (at 150–210 °C) corresponds to the temperature of the fastest decrease of relative resistivity changes. It is seen that the Sc,Zr-addition has almost no effect on microhardness changes up to  $\sim 240^\circ\text{C}$ . However, after that, the HV values of the alloy with the Sc,Zr-addition after only slight decrease reach an indistinctive local maximum at  $\sim 400^\circ\text{C}$  in contrast to the continual HV value decrease in AlZnMg alloy. The  $\Delta\text{HV}$  difference between AlZnMg and AlZnMgScZr alloys at the end of annealing is nearly HV  $\approx 20$ . Figure 1b shows the DSC curves of the MC alloys at a heating rate of 1 K min $^{-1}$  up to 350 °C. The first endothermic effect (labelled process A) is followed by a significant exothermic effect (process B). One can see two insignificant exothermic processes at temperatures above  $\sim 200^\circ\text{C}$  (labelled as processes C and

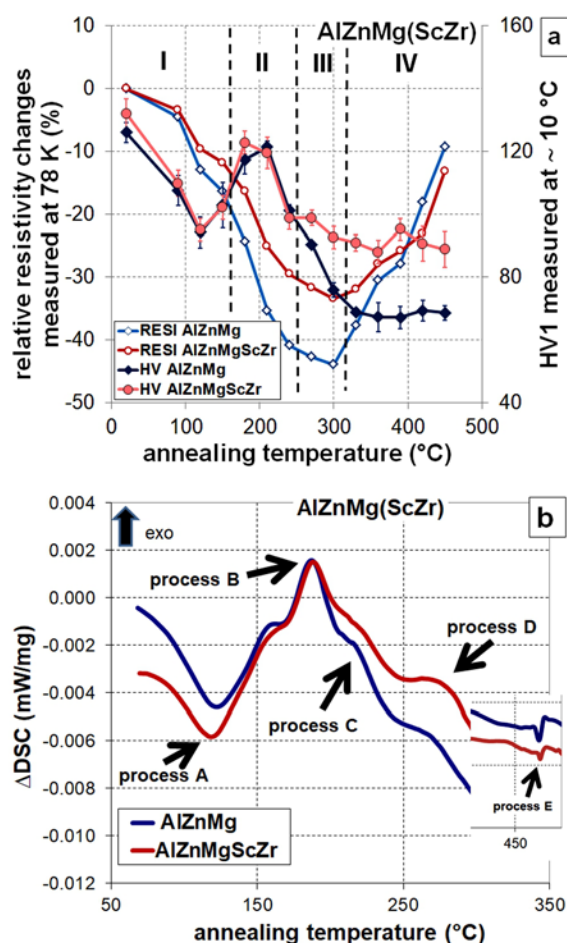


Fig. 1. AlZnMg(ScZr) alloy in the MC state: a) isochronal annealing curves of relative resistivity changes and microhardness HV1 with standard deviation, b) DSC curves for linear heating rate 1 K min<sup>-1</sup> (inset 20 K min<sup>-1</sup> at a temperature ~ 475 °C).

D). No other thermal effects were observed up to the end of the linear heating at the heating rates of 1, 2, 5, 10 and 30 K min<sup>-1</sup> up to 450 °C. The character of these processes agrees very well with DSC results observed in [3, 6, 8, 10].

SEM proved the Zn,Mg-containing eutectic phase at grain boundaries in the MC state of both alloys. An overview of the AlZnMgScZr alloy in the MC state is shown in Fig. 2. The melting (process E) of this eutectic phase was observed at ~ 475 °C (Fig. 1b – see inset) in the DSC curves at a heating rate of 20 K min<sup>-1</sup> which was performed up to 500 °C. It was also observed in the initial state by SEM and TEM that the Sc,Zr-content in the AlZnMgScZr alloy is not homogeneously distributed but concentrated in randomly localized matrix regions and together with Zn and Mg in the particles enclosed with the eutectic phase at grain boundaries. The only small density of dislocations in grain interiors in the MC state of the alloys was observed by TEM. No other phases and/or par-

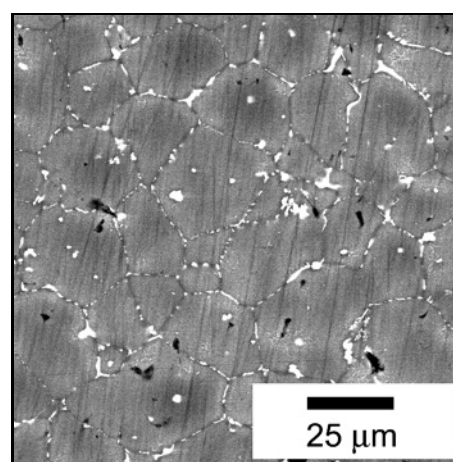


Fig. 2. SEM image of the AlZnMgScZr alloy in the MC state.

ticles (except the mentioned eutectic phase) were detected.

The ageing processes in the alloys of the Al-Zn-Mg-based system are complex, and the decomposition of saturated solid solutions obtained by quenching takes place in several stages [5, 6]. Typically, the formation of coherent Guinier-Preston (GP) zones and/or Zn,Mg-rich clusters precedes the formation of the semicoherent intermediate precipitates and incoherent equilibrium precipitates [2–8, 16]. In general, the early precipitation stages can be universally abundant in Al-based alloys and are known to affect the resistivity and (micro)hardness [19–21]. Many authors have attempted to explain changes of electrical resistivity and microhardness at the beginning of the precipitation kinetics in the Al-based alloys due to the formation of the GP zones and/or clusters [8, 19–21]. Preliminary positron annihilation spectroscopy (PAS) measurements in the AlZnMg alloy show that the positrons annihilate at traps associated with GP zones and/or small clusters and are characterized by a positron lifetime of 0.213 ns. This measured value is in a good agreement with the results in [22] and corresponds to the positrons annihilations from GP zones. From a comparison of the isochronal annealing curves of the studied MC alloys up to ~ 150 °C (Fig. 1a), it can be concluded that the GP zones and/or Zn,Mg-rich clusters are dissolved first. This dissolution is responsible for the resistivity I-stage and microhardness decrease. The first endothermic thermal effect (process A – see Fig. 1b) in both alloys up to ~ 150 °C corresponds to the dissolution of GP zones and/or Zn,Mg-rich clusters, too. These results are consistent to the DSC measurements of the AA7012 (Al-Zn-Mg-Cu-Zr) alloy (see [23]) where the first endothermic effect appears at temperatures ranging from 90 to 140 °C depending on the scanning rate; this peak refers to the dissolution of a pre-precipitated phase

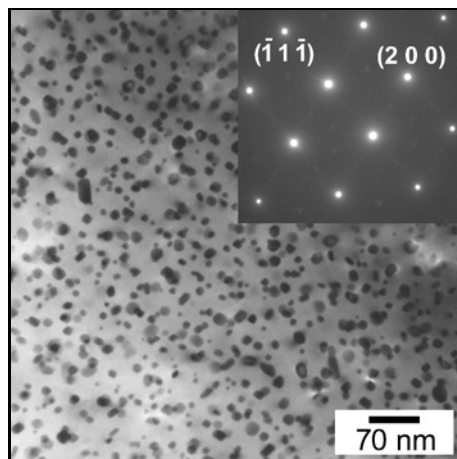


Fig. 3. TEM image of the AlZnMg alloy in the MC state isochronally annealed up to 210°C showing particles of the  $\eta'$ -phase. See the corresponding ED in the inset, [0 1 1] Al zone.

(GP zones and/or clusters) produced during the natural ageing and indicates that this dissolution phenomenon is thermally activated [23]. The formation of the GP zones and/or Zn,Mg-rich clusters in the studied alloys was probably done while cooling the material after casting and subsequent storage at room temperature (RT). In comparison with the AlZnMg alloy, there is no observable effect on the formation of GP zones and/or Zn,Mg-rich clusters during the isochronal (i.e., non-isothermal) annealing considering the small concentration of the Sc and Zr atoms dissolved in the matrix. It is probably due to the large content of these additions in the Zn,Mg-rich particles around grain boundaries in the AlZnMgScZr alloy.

Figure 3 shows the TEM image of the AlZnMg alloy in the MC state isochronally annealed up to 210°C, where the dense dispersion of the metastable  $\eta'$ -phase particles can be seen. Thus the main resistivity decrease (II-stage) and microhardness increase in the temperature range of 150–210°C and significant exothermal process B in both alloys studied are due to the precipitation of these particles. In the Al-Zn-Mg(-Cu)-based alloys the metastable  $\eta'$ -phase is a typical hardening phase [4–6]. It can also be concluded that the Sc,Zr-addition does not significantly influence the precipitation of the metastable  $\eta'$ -phase particles in the MC alloy.

After annealing up to 360°C, the microstructure observation of both alloys proved the presence of the particles with Mn,Fe-content, stable  $\eta$ -phase and probably  $T$ -phase ( $\text{Al}_2\text{Zn}_3\text{Mg}_3$ ), as detected by EDS (see Fig. 4). Mn and Fe addition is traditionally contained in commercial alloys of the AA7xxx series [1]. Precipitation of the  $T$ -phase and Mn,Fe-containing phase does not lead to the hardening [5–9]. The precip-

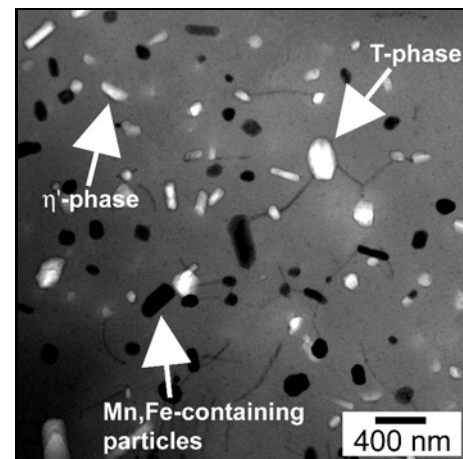


Fig. 4. Bright field TEM image of AlZnMgScZr alloy in the MC state isochronally annealed up to 360°C. See Mn,Fe-containing particles (dark needles), particles of the  $\eta$ -phase (bright needles) and probable particles of the  $T$ -phase (large bright particles).

itation of the  $T$ -phase was also observed in the alloys of the same composition in cold-rolled state at comparable temperature range [24]. It can be mentioned that the AlZnMgScZr alloy shows higher HV values at temperatures above  $\sim 270^\circ\text{C}$  in contrast to the AlZnMg alloy (see Fig. 1a). One can conclude that this result is probably connected with the Sc,Zr-addition. The hardening effect at this temperature range is typical for the Al-Sc-Zr-based alloys [1, 11–13, 18]. However, the existence of the  $\text{Al}_3(\text{Sc,Zr})$ -phase particles was not observed directly (by TEM) as the consequence of the small amount of these additions in the matrix and/or their inhomogeneous distribution such as randomly localized matrix regions with the higher Sc,Zr-content. This is probably the reason of relatively small hardening ( $\Delta\text{HV} \sim 15$ ) in comparison with the typical hardening effect ( $\Delta\text{HV} \sim 40$ ) in the Al-Sc-Zr-based alloys [12, 13, 18]. It is mentioned that the  $\text{Al}_3(\text{Sc,Zr})$ -phase particles were observed in the heat-treated state in this temperature range (see Chapter 3.3 below). This justifies the assumption that the precipitation takes place at temperatures above  $\sim 300^\circ\text{C}$  also in the MC state of the alloy.

The small heat effects (processes C and D) are probably related to the observed formation of the particles of the stable  $\eta$ -phase and  $T$ -phase. The temperature region corresponds very well to the observation of the others where precipitation of the metastable  $\eta'$ -phase is immediately followed by precipitation of the  $\eta$ -phase and  $T$ -phase as well as with the temperature range of the simulated fraction evolution of these phases for the pure Al-Zn-Mg alloy during the DSC run [3, 8]. The particle precipitation of the Mn,Fe-containing phase is probably the reason for the un-  
dulating of the resistivity curves (Fig. 1a) at tempera-

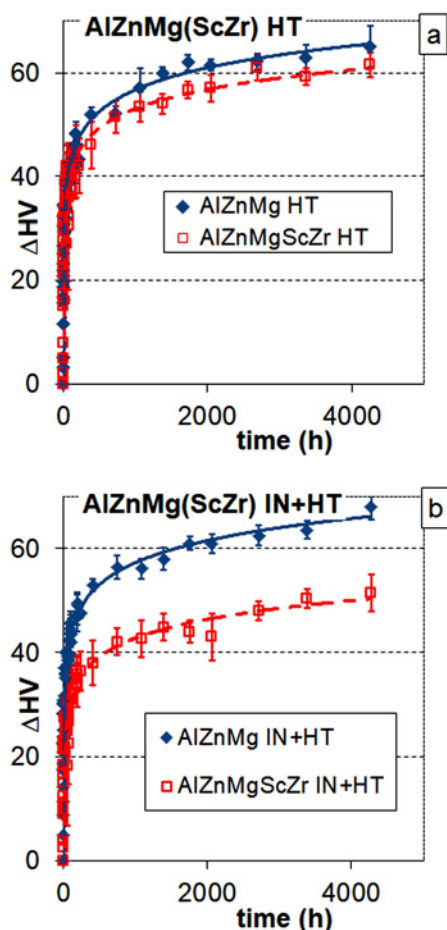


Fig. 5. Microhardness  $\Delta HV$  development of the AlZnMg(ScZr) alloys during natural ageing: a) in the HT state, b) IN+HT state.

tures above 330 °C. This process can also be affected by weak anticipated precipitation of the  $Al_3(Sc,Zr)$ -phase particles in the AlZnMgScZr alloy.

Annealing above 390 °C gradually led to the dissolution of the particles from the Al-Zn-Mg system. Furthermore, the eutectic Zn,Mg-containing phase partly disappeared during the isochronal annealing above this temperature as it was observed by SEM (not shown). These effects are mainly connected with the resistivity increase above  $\sim 360$  °C in both alloys studied.

### 3.2. Natural ageing of the heat-treated alloys

Figure 5 shows the development of the microhardness changes  $\Delta HV$  during NA in the HT and IN+HT alloys. HV values increase immediately from the beginning of NA. The initial microhardness values of the HT alloys ( $HV \approx 67$  for the AlZnMg and  $HV \approx 80$  for the AlZnMgScZr) and IN+HT alloys ( $HV \approx 70$  for the AlZnMg and  $HV_{0.5} \approx 90$  for the AlZnMgScZr) are significantly lower than in the MC state. The HV values

reflect the Sc,Zr-addition in the alloys.

PAS investigations in the Al-based alloys indicate that the interaction between solute atoms and vacancies has a significant effect on pre-precipitated phase (e.g., GP zones and/or clusters formation) [21, 25]. There has been a controversy in the literature regarding the chemistry of the pre-precipitated phases [2–8, 25] in the Al-Zn-Mg-based alloys. Some authors suggest that they are Zn and/or Zn-vacancy clusters, but others suggest that they contain both Zn and Mg atoms or the mixture of Al, Zn and Mg atoms. Parallel to the PAS observation in the Al-Mg-Si-based alloys [21, 25–27], one can conclude that immediately after quenching the Al-Zn-Mg-based alloy contains vacancies associated with single and/or multiple Zn- and/or Mg-clusters and/or Zn,Mg-co-clusters developed during quenching and in the course of further NA. Solute agglomerates containing vacancies are gradually transformed into vacancy-free GP zones releasing vacancies which disappear by diffusion into sinks. Owing to the strengthening effect of the GP zones and/or clusters, the microhardness values of the alloys increase continuously during ageing at RT after quenching due to the solute clusters growing and GP zones formation in agreement with the others for the Al-Zn-Mg-based alloys (e.g. [19, 20]).

The initial rate of hardening is comparable up to  $\sim 1000$  hours in the HT alloys and only up to  $\sim 50$  hours in the IN+HT alloys (see Fig. 5), respectively. It seems probable that the microhardness changes during NA of the alloys studied are influenced by the addition of Sc and Zr and precipitation of the  $Al_3(Sc,Zr)$ -phase particles during annealing at 300 °C, respectively. The effect of Sc in the Al-Zn-Mg system was studied by several authors with controversial results concerning the question of whether the addition of Sc accelerates or retards the decomposition of the supersaturated solid solution of the Al-Zn-Mg system. The mentioned controversy in the literature may originate from observations in different stages of the ageing process (there was a different content of Zn and Mg or Cu-addition in some materials [19, 20]). On the other hand, GP zone formation occurs at RT which is only possible if diffusion is assisted with a substantial amount of non-equilibrium quenched-in vacancies [28]. Authors of this study also showed via PAS in the Al-(Mn)-Sc-Zr alloy that positrons are trapped at vacancy-like defects associated with Sc atoms and/or Sc-rich clusters [18]. Concerning the different microhardness changes during NA in the Sc,Zr-containing alloys one can conclude that the vacancy concentration can also be influenced in the alloys studied. However, the microstructure observation by TEM of the alloys in the HT as well as IN+HT state showed only the presence of the particles of the (meta)stable phase of the Al-Zn-Mg system with comparable volume fraction. An overview of the microstructure of the AlZnMgScZr alloy in the

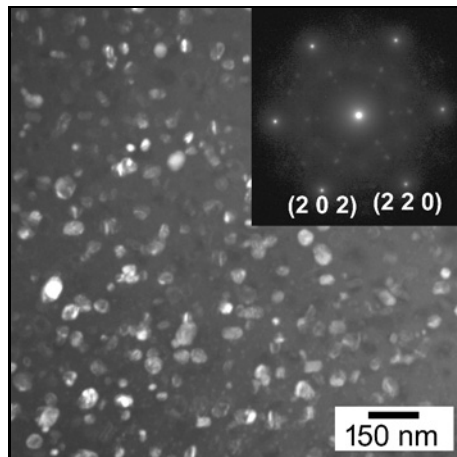


Fig. 6. TEM image of the AlZnMgScZr alloy in the IN+HT state. Weak diffraction spots in  $[\bar{1}1\bar{1}]$  Al zone diffractogram mainly from the  $\eta'$ - and/or  $\eta$ -phase.

IN+HT state is shown in Fig. 6, weak diffraction spots in  $[\bar{1}1\bar{1}]$  Al zone diffractogram (see inset – Fig. 6) are either of  $\eta'$ - and/or  $\eta$ -phase. Diffuse spots in the middle of  $\{2-20\}$  Al matrix spots indicate a possibility of the  $\text{Al}_3(\text{Sc,Zr})$ -phase particle precipitation. However, the diffraction spot observed in the middle of  $\{113\}$  Al matrix spots in  $[-211]$  Al zone cannot be ascribed to this phase at all. However, excluding precipitation of the  $\text{Al}_3(\text{Sc,Zr})$ -phase particles completely would not be correct. No  $\text{Al}_3(\text{Sc,Zr})$ -phase particles were observed directly in the Sc,Zr-containing alloys probably as a consequence of inhomogeneous distribution. This was confirmed by SEM observation where Sc-rich regions were visible. The eutectic structure, very similar to the initial state in the all alloys studied, was observed after the heat treatment. However, the difference of the HV values after HT as well as IN+HT treatment indicates that besides the weak precipitation of the (meta)stable phase of the Al-Zn-Mg the weak precipitation (especially during annealing at 300 °C) of the  $\text{Al}_3\text{Sc}$ - and/or  $\text{Al}_3(\text{Sc,Zr})$ -phase particles probably also takes place. One can also conclude that the HT, as well as IN+HT annealing, is insufficient for general homogenization of the Al-Zn-Mg system.

### 3.3. Phase development in the heat-treated alloys during isochronal annealing

The resistivity and microhardness isochronal curves for the HT and IN+HT+NA alloys are given in Fig. 7. The electrical resistivity curves of the HT alloys show a significant increase of the  $\Delta\rho/\rho_0$  (I-stage up to  $\sim 150^\circ\text{C}$ ) followed by resistivity decrease (II-stage between 150 and 240 °C, III-stage between 240 and 300 °C) to a minimum. Then the electrical resistivity of both alloys increases (IV-stage). The microhard-

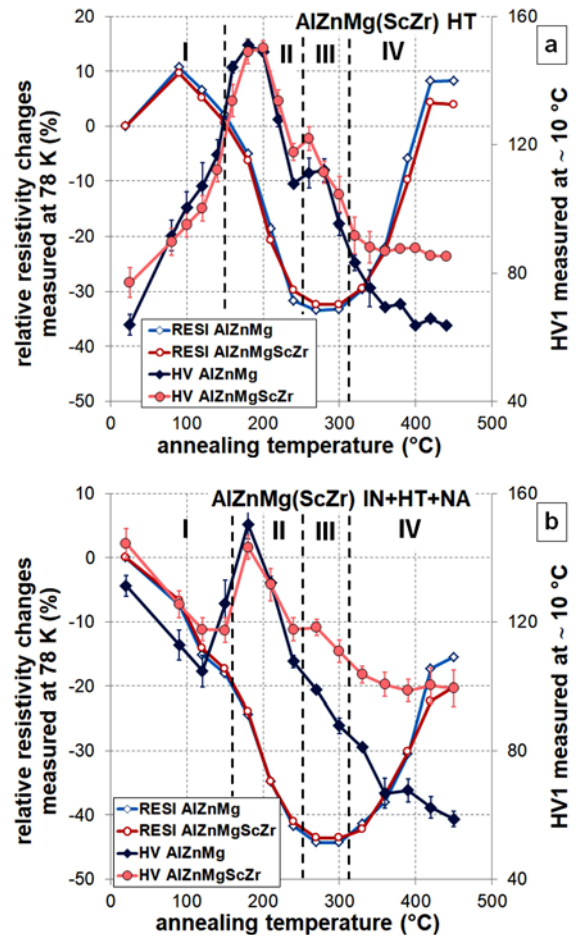


Fig. 7. Isochronal annealing curves of relative resistivity changes (measured at 78 K) and microhardness HV (measured at RT) with standard deviation: a) in the HT state, b) IN+HT+NA state.

ness values of the HT alloys are comparable for both alloys up to  $\sim 300^\circ\text{C}$ . The HT alloys reach a maximal hardening at  $\sim 180\text{--}200^\circ\text{C}$ . The temperature range of the hardening peak corresponds to the temperature of the fastest decrease of relative resistivity changes. It can be seen that the Sc,Zr-addition has almost no effect on microhardness changes up to 330 °C. The relative resistivity changes of the IN+HT+NA alloys show a significant decrease of the  $\Delta\rho/\rho_0$  in three stages (I-stage up to  $\sim 150^\circ\text{C}$ , II-stage between 150 and 210 °C, III-stage between 210 and 300 °C). Then the electrical resistivity increases (IV-stage). The initial microhardness HV values of the IN+HT+NA alloys are higher than those of the HT alloys due to the presence of the  $\eta'$ -phase particles developed during the heat treatment and GP zones and/or clusters developed during subsequent natural ageing. The higher HV value of the AlZnMgScZr alloy in the IN+HT+NA state is probably caused by possible precipitation of the Sc,Zr-containing particles during the treatment. The temperature range of the hardening

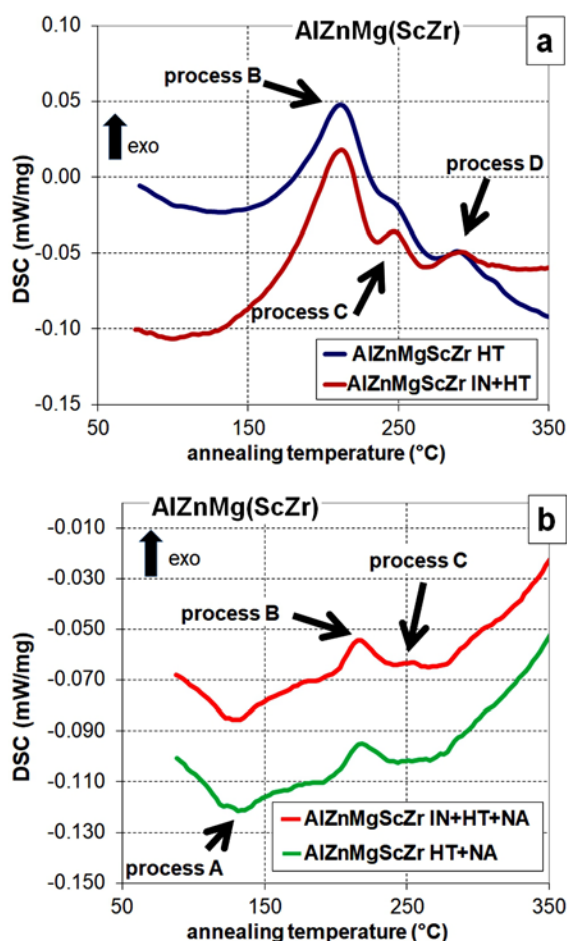


Fig. 8. DSC curves (heating rate of  $5 \text{ K min}^{-1}$ ) of the AlZnMgScZr alloy: a) HT, IN+HT, b) HT+NA, IN+HT+NA state.

peak of IN+HT+NA alloys corresponds to the temperature of the fastest decrease of relative resistivity changes. Microhardness development of all alloys studied also reflects the Sc,Zr-addition at temperatures above  $\sim 300^\circ\text{C}$ .

Although the electrical resistivity and microhardness measurements were done only in HT and IN+HT+NA alloys, DSC measurements were done on multiple combinations of the heat treatment. Figure 8 shows the DSC curves of the AlZnMgScZr alloy in the HT, HT+NA, IN+HT, and IN+HT+NA state at a heating rate of  $5 \text{ K min}^{-1}$  up to  $350^\circ\text{C}$ . This rate was chosen for visibility reasons of the observed thermal processes (labelled as A–D). No other thermal effects were observed up to the end of the linear heating. DSC measurements of the AlZnMg alloy were very similar to the alloy with Sc,Zr-addition. The thermal response and activation energies of the observed processes are discussed in the following section (see Chapter 3.4. below).

From a comparison of the annealing curves of the studied alloys up to  $\sim 150^\circ\text{C}$  (Figs. 1 and 7), it can be

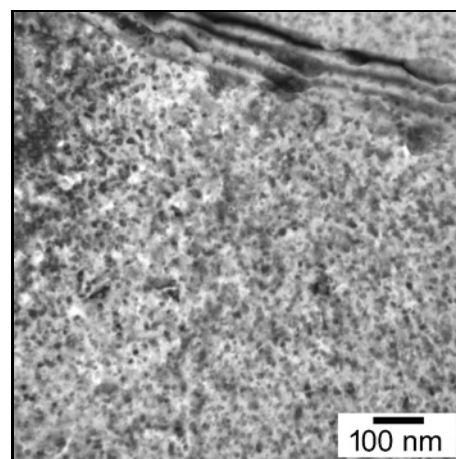


Fig. 9. TEM image of the AlZnMgScZr alloy in the IN+HT state isochronally annealed up to  $210^\circ\text{C}$ .

concluded that the GP zones and/or Zn,Mg-rich clusters are formed in the HT alloys during the isochronal annealing. This process is connected with microhardness and electrical resistivity increase at I-stage. On the contrary, the GP zones and/or Zn,Mg-rich clusters are dissolved first at this temperature range (process A) in the HT+NA and IN+HT+NA alloys. This dissolution leads to the resistivity (I-stage) and microhardness decrease. Thus the first endothermic thermal effect (process A – see Fig. 8b) in the HT+NA as well as IN+HT+NA alloys up to  $\sim 150^\circ\text{C}$  corresponds to the dissolution of GP zones and/or comparable to the MC state (compare Figs. 1b and 8b). Note that the DSC measurements in the present work did not start to measure at RT but at  $\sim 80^\circ\text{C}$ , and the sensitivity of our apparatus was not high enough to detect the exothermic effect caused by GP zones formation in the HT and IN+HT alloys.

TEM observation at  $210^\circ\text{C}$  proved a fine and dense dispersion of the  $\eta'$ -phase particles (Fig. 9) in the AlZnMgScZr alloy in the IN+HT state. Thus the fastest resistivity decrease (II-stage) and microhardness increase of the all alloys studied in the temperature range of  $150\text{--}210^\circ\text{C}$  is due to additional precipitation of the metastable  $\eta'$ -phase particles. The significant exothermic effect (process B) in DSC curves (see Fig. 8) can be ascribed to this process, too. It can also be concluded that the precipitation of the metastable  $\eta'$ -phase particles in the non-natural aged (HT and IN+HT) alloys is more pronounced and shifted to the lower temperatures ( $\sim 10^\circ\text{C}$ ) in comparison to the HT+NA and IN+HT+NA alloys as the consequence of higher supersaturation of the Al-Zn-Mg system.

TEM of the alloys isochronally annealed up to  $360^\circ\text{C}$  observed the presence of the coarsened  $\eta$ -phase and probably of the  $T$ -phase particles (see Fig. 10a). The similar microstructure was observed by the others, see [5, 24, 29], at this temperature range. In par-

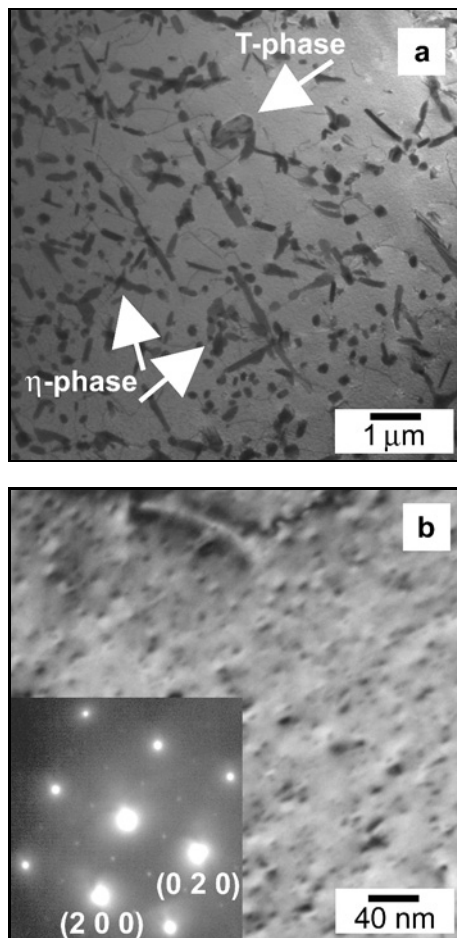


Fig. 10. TEM image of the AlZnMgScZr alloy in the IN+HT state isochronally annealed up to 360 °C: a) particles of the  $\eta$ -phase and  $T$ -phase, b) the  $\text{Al}_3(\text{Sc,Zr})$ -phase particles with  $L1_2$  structure (ED pattern of [001] Al zone in the inset).

allel to the MC state (compare DSC curves in Fig. 1b and Fig. 8), it can be assumed that the precipitation of the  $T$ -phase (process D in DSC curves in Fig. 8) takes place also in the heat-treated alloys during the annealing up to  $\sim 300^\circ\text{C}$ . The temperature region corresponds very well to the observation of the others where precipitation of the stable  $\eta$ -phase is immediately followed by precipitation of the  $T$ -phase [3]. The markedness of the maximum heat flow of these effects in the alloys without natural ageing was higher as a consequence of the higher oversaturation of Zn and Mg atoms. The particle precipitation of the  $\eta$ -phase and  $T$ -phase is a probable explanation of the subsequent resistivity decrease (III-stage) and undulating of the HV microhardness curves at a temperature range of 210–300 °C (Fig. 7). The resistivity increase at temperatures above 300 °C corresponds mainly to the dissolution of the particles of the Al-Zn-Mg system. Assuming the presence of the Sc,Zr-containing particles, it can also be concluded that the yield strength of the AlZnMgScZr alloys cannot be expressed as a

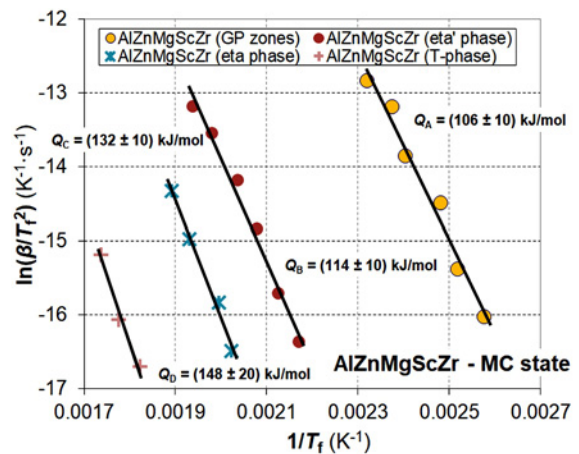


Fig. 11. Kissinger plot constructed from series of DSC measurements of the AlZnMgScZr alloy in the MC state with various heating rates 1–30  $\text{K min}^{-1}$ .

linear superposition of several strength contributions. This conclusion is in agreement with the observation of the others in the commercial AA6xxx alloys, see [30, 31]. The AlZnMgScZr alloys show significantly higher HV values at higher temperatures in contrast to the AlZnMg alloys (Fig. 7). Although the  $\text{Al}_3(\text{Sc,Zr})$ -phase particles were not directly observed in the earlier cases (see above), these particles in the IN+HT alloy isochronally annealed up to 360 °C were detected (see Fig. 10b). The particles in the alloy exhibit a typical “coffee bean” contrast. That is the reason for better hardening of the AlZnMgScZr alloys (Fig. 7). This also allows us to assume that the  $\text{Al}_3(\text{Sc,Zr})$ -phase precipitation is going on in this temperature range also in the MC alloy (see Chapter 3.1).

### 3.4. Thermal properties of the AlZnMg(ScZr) alloys

To obtain information on the kinetics of the phase formation in the alloys studied in the different states (MC, HT, IN+HT, HT+NA, IN+HT+NA), we examined the apparent activation energy of thermal processes by using DSC. One endothermic process marked A, and three exothermic processes marked B–D (see Figs. 1 and 8) were observed in the DSC curves of the samples. The effect A obviously corresponds to the dissolution of GP zones and/or clusters, effects B and C to the precipitation of the metastable  $\eta'$ -phase and stable  $\eta$ -phase particles, respectively. The effect D probably corresponds to the precipitation of the  $T$ -phase particles. The melting of the eutectic phase (process E at a heating rate of 20  $\text{K min}^{-1}$ ) was observed at  $\sim 475^\circ\text{C}$  (see Fig. 1b). DSC curves measured with various heating rates were used for the determination of activation energies of the thermal processes A–D. Figure 11 shows the example of the Kissinger plot [32] for the AlZnMgScZr alloy in the MC state,

Table 1. Activation energies  $Q$  of the processes A–D determined by the Kissinger analysis of DSC data for all alloys studied

Sample	Process	Activation energy $Q$ (kJ mol <sup>-1</sup> )
MC	A (GP zones dissolution)	AlZnMg: 112 ± 15 AlZnMgScZr: 106 ± 10
	B ( $\eta'$ -phase particles)	AlZnMg: 111 ± 8 AlZnMgScZr: 114 ± 10
	C ( $\eta$ -phase particles)	AlZnMg: 130 ± 8 AlZnMgScZr: 132 ± 10
	D ( $T$ -phase particles)	AlZnMg: 142 ± 14 AlZnMgScZr: 148 ± 20
HT	B ( $\eta'$ -phase particles)	AlZnMg: 113 ± 8 AlZnMgScZr: 112 ± 8
	C ( $\eta$ -phase particles)	AlZnMg: 126 ± 4 AlZnMgScZr: 121 ± 4
	D ( $T$ -phase particles)	AlZnMg: 140 ± 10 AlZnMgScZr: 151 ± 8
HT+NA	A (GP zones dissolution)	AlZnMg: 107 ± 8 AlZnMgScZr: 103 ± 7
	B ( $\eta'$ -phase particles)	AlZnMg: 106 ± 6 AlZnMgScZr: 109 ± 6
	C ( $\eta$ -phase particles)	AlZnMg: 123 ± 6 AlZnMgScZr: N/A
	D ( $T$ -phase particles)	N/A
IN+HT	B ( $\eta'$ -phase particles)	AlZnMg: 111 ± 4 AlZnMgScZr: 112 ± 12
	C ( $\eta$ -phase particles)	AlZnMg: 124 ± 6 AlZnMgScZr: 123 ± 4
	D ( $T$ -phase particles)	AlZnMg: 143 ± 6 AlZnMgScZr: 139 ± 8
IN+HT+NA	A (GP zones dissolution)	AlZnMg: 103 ± 8 AlZnMgScZr: 108 ± 7
	B ( $\eta'$ -phase particles)	AlZnMg: 109 ± 8 AlZnMgScZr: 111 ± 4
	C ( $\eta$ -phase particles)	N/A
	D ( $T$ -phase particles)	N/A

i.e.,  $\ln(\beta/T_f^2)$  plotted versus  $1/T_f$ , where  $T_f$  is the characteristic temperature of a DSC peak and  $\beta$  is the

heating rate. One can see that each effect obeys the Arrhenius law and is represented by a straight line

in the Kissinger plot. The activation energies determined by linear regression of the experimental data for the all studied alloys are listed in Table 1. Some energies were not calculated as a consequence of the low markedness of the maximum heat flow (e.g., for the natural-aged alloys). The markedness of the maximum heat flow of the B–D processes in the HT and IN+HT alloys was higher than in the HT+NA as well as IN+HT+NA alloys as a consequence of the higher oversaturation of Zn and Mg atoms. Although some effects were not evaluated due to small distinctness, it can be seen that DSC measurements are in a very good agreement with the resistivity and microhardness results.

The average activation energy for the dissolution of the GP zones (process A) determined for the MC, HT+NA and IN+HT+NA samples in the present work is calculated  $\sim 106 \text{ kJ mol}^{-1}$  (see Table 1). The calculated range of the activation energy for the dissolution of the GP zones is higher than that for the GP zones formation ( $\sim 60 \text{ kJ mol}^{-1}$  [33]) in the Al-Mg-Zn-based alloys. The activation energies for the GP zones dissolution reported in literature exhibit a large scatter and cover a wide range from 65–120  $\text{kJ mol}^{-1}$  [23, 24, 33, 34]. This is because of this DSC peak that can be overlapped by the previous formation of these zones. It has to be noted that a weak exothermic effect was reported to occur in solution-treated Al-Zn-Mg-based alloys at low temperatures 30–110 °C [5, 19, 29] – this peak was attributed to clustering of solutes and/or formation of the GP zones.

The activation energy of the  $\eta'$ -phase precipitation (process B) in the studied alloys was calculated as  $\sim 111 \text{ kJ mol}^{-1}$ . The activation energies of the  $\eta'$ -phase precipitation are comparable through the materials studied independently on the annealing and Sc,Zr-addition. The value agrees within accuracy with the apparent activation energy for the precipitation of the  $\eta'$ -phase (80–120  $\text{kJ mol}^{-1}$ ) determined in the Al-Zn-Mg-based alloys after ageing at various temperatures [5, 6, 22, 23, 33]. Note that the activation energy of the dissolution of the GP zones and precipitation of the  $\eta'$ -phase particles in the cold-rolled AlZnMg and AlZnMgScZr alloys was published by the authors in previous work as  $(105 \pm 20) \text{ kJ mol}^{-1}$  and  $(110 \pm 10) \text{ kJ mol}^{-1}$ , respectively [24]. The obtained values are comparable to the diffusion activation energies of both Zn and Mg in Al of  $\sim 120 \text{ kJ mol}^{-1}$  [33].

The activation energy for the  $\eta$ -phase formation (process C) in the alloys is calculated as  $\sim 126 \text{ kJ mol}^{-1}$ . This value is in good agreement (115–160  $\text{kJ mol}^{-1}$ ) with literature – see [23, 33]. The activation energy for the precipitation of the  $\eta$ -phase seems to be lower for the alloys after heat-treatment, but it is comparable in all alloys taking into account experimental uncertainties.

Consequently, a weak thermal process D was detected only for some heating rates of some studied alloys. The effect corresponds to the additional weak precipitation of the precipitation of the  $T$ -phase particles. The activation energy of this process was obtained as  $\sim 144 \text{ kJ mol}^{-1}$ . The calculated energy of this process is encumbered by a big scatter due to the small thermal response. Although the data in the literature for this precipitation are not available, the calculated value indicates that precipitation of the  $T$ -phase is more difficult than the precipitation of the stable  $\eta$ -phase.

#### 4. Conclusions

From the results of the microstructural observation and mechanical, electrical and thermal properties of the Al-Zn-Mg(-Mn,Fe) alloy with and without Sc and Zr addition, it can be concluded:

- The distinct changes in resistivity and microhardness curves as well as in heat flow of the alloys studied are mainly caused by dissolution of the Zn,Mg-containing Guinier-Preston (GP) zones and subsequent precipitation of the particles from the Al-Zn-Mg system.

- The hardening effect after isochronal annealing at temperatures above  $\sim 280 \text{ °C}$  reflects the Sc,Zr-addition. Precipitation of the Mn,Fe-containing particles was also observed in the alloy with Sc and Zr addition. Precipitation of these particles as well as of the  $\eta$ - and  $T$ -phase particles does not influence hardening significantly.

- Microstructure observation proved the Zn,Mg-containing eutectic phase at grain boundaries in the alloys studied. Sc,Zr-content is mainly concentrated in randomly-localized regions in the Al matrix. Melting of the eutectic phase was observed at  $\sim 475 \text{ °C}$ .

- Heat treatment at 300 °C for 60 min and subsequently 460 °C for 45 min is insufficient for usual homogenization of the Al-Zn-Mg system.

- Strengthening effect due to the formation of the GP zones and/or growing of the clusters is observed during natural ageing. Sc and Zr addition can influence the vacancy concentration in the alloys studied.

- The apparent activation energy values were calculated as dissolution of the GP zones ( $\sim 106 \text{ kJ mol}^{-1}$ ), formation of the metastable  $\eta'$ -phase ( $\sim 111 \text{ kJ mol}^{-1}$ ), formation of the stable  $\eta$ -phase ( $\sim 126 \text{ kJ mol}^{-1}$ ) and formation of the  $T$ -phase ( $\sim 144 \text{ kJ mol}^{-1}$ ).

#### Acknowledgement

This work was supported by The Czech Science Foundation (GACR, project no. 17-17139S).

## References

- [1] Toropova, L. S., Eskin, D. G., Kharakterova, M. L., Dobatkina, T. V.: Advanced Aluminium Alloys Containing Scandium – Structure and Properties. The Netherlands, Gordon and Breach Science Publisher 1998.
- [2] Chen, S., Jiyu L., Gui-Yun, H., Kanghua, C., Lanping, H.: Journal of Alloys and Compounds, 757, 2018, p. 259. [doi:10.1016/j.jallcom.2018.05.063](https://doi.org/10.1016/j.jallcom.2018.05.063)
- [3] Lang, P., Wojcik, T., Povoden-Karadeniz, E., Falaha, A., Kozeschnik, E.: Journal of Alloys and Compounds, 609, 2014, p. 129. [doi:10.1016/j.jallcom.2014.04.119](https://doi.org/10.1016/j.jallcom.2014.04.119)
- [4] Prasanta, K. R., Ghosh, M. M., Ghosh, K. S.: Materials Characterization, 104, 2015, p. 49. [doi:10.1016/j.matchar.2015.03.025](https://doi.org/10.1016/j.matchar.2015.03.025)
- [5] Ghosh, K. S., Gao, N., Starink, M. J.: Materials Science and Engineering: A, 552, 2012, p. 164. [doi:10.1016/j.msea.2012.05.026](https://doi.org/10.1016/j.msea.2012.05.026)
- [6] Ghosh, K. S., Gao, N.: Transactions of Nonferrous Metals Society of China, 21, 2011, p. 1199. [doi:10.1016/S1003-6326\(11\)60843-1](https://doi.org/10.1016/S1003-6326(11)60843-1)
- [7] Starink, M. J., Wang, S. C.: Acta Materialia, 51, 2003, p. 5131. [doi:10.1016/S1359-6454\(03\)00363-X](https://doi.org/10.1016/S1359-6454(03)00363-X)
- [8] Tang, J., Chen, H., Zhang, X., Liu, X., Liu, W., Ouyang, H., Li, H.: Transactions of Nonferrous Metals Society of China, 22, 2012, p. 1255. [doi:10.1016/S1003-6326\(11\)61313-7](https://doi.org/10.1016/S1003-6326(11)61313-7)
- [9] Yang, X. B., Chen, J. H., Liu, J. Z., Qin, F., Xie, J., Wu, C. L.: Journal of Alloys and Compounds, 610, 2014, p. 69. [doi:10.1016/j.jallcom.2014.04.185](https://doi.org/10.1016/j.jallcom.2014.04.185)
- [10] Sha, G., Cerezo, A.: Acta Materialia, 52, 2004, p. 4503. [doi:10.1016/j.actamat.2004.06.025](https://doi.org/10.1016/j.actamat.2004.06.025)
- [11] Vo, N. Q., Dunand, D. C., Seidman, D. N.: Materials Science and Engineering: A, 677, 2016, p. 485. [doi:10.1016/j.msea.2016.09.065](https://doi.org/10.1016/j.msea.2016.09.065)
- [12] Vlach, M., Stulikova, I., Smola, B., Kekule, T., Kudrnova, H., Kodetova, V., Ocenasek, V., Malek, J., Neubert, V.: Kovové Materiály-Metallic Materials, 53, 2015, p. 295. [doi:10.4149/km-2015-5-295](https://doi.org/10.4149/km-2015-5-295)
- [13] Kolar, M., Ocenasek, V., Uhlir, J., Stuliková, I., Smola, B., Vlach, M., Neubert, V., Sperlink, K.: Materials Science Forum, 567–568, 2008, p. 357. [doi:10.4028/www.scientific.net/MSF.567-568.357](https://doi.org/10.4028/www.scientific.net/MSF.567-568.357)
- [14] Teng, G. B., Liu, C. Y., Ma, Z. Y., Zhou, W. B., Wei, L. L., Chen, Y., Li, J., Mo, Y. F.: Materials Science and Engineering: A, 713, 2018, p. 61. [doi:10.1016/j.msea.2017.12.067](https://doi.org/10.1016/j.msea.2017.12.067)
- [15] Senkov, O. N., Shagiev, M. R., Senkova, S. V., Miracle, D. B.: Acta Materialia, 56, 2008, p. 3723. [doi:10.1016/j.actamat.2008.04.005](https://doi.org/10.1016/j.actamat.2008.04.005)
- [16] Liu, J., Yao, P., Zhao, N., Shi, C., Li, H., Xi, D., Yang, S.: Journal of Alloys and Compounds, 657, 2016, p. 717. [doi:10.1016/j.jallcom.2015.10.122](https://doi.org/10.1016/j.jallcom.2015.10.122)
- [17] Li, B., Pan, Q., Shi, Y., Li, C., Yin, Z.: Transactions of Nonferrous Metals Society of China, 23, 2013, p. 3568. [doi:10.1016/S1003-6326\(13\)62902-7](https://doi.org/10.1016/S1003-6326(13)62902-7)
- [18] Vlach, M., Cizek, J., Melikhova, O., Stulikova, I., Smola, B., Kekule, T., Kudrnova, H., Gemma, R., Neubert, V.: Metallurgical and Materials Transactions A, 46, 2015, p. 1556. [doi:10.1007/s11661-015-2767-x](https://doi.org/10.1007/s11661-015-2767-x)
- [19] Chinh, N. Q., Lendvai, J., Ping, D. H., Hono, K.: Journal of Alloys and Compounds, 378, 2004, p. 52. [doi:10.1016/j.jallcom.2003.11.175](https://doi.org/10.1016/j.jallcom.2003.11.175)
- [20] Dellah, M., Bournane, M., Ragab, K. A., Sadaoui, Y., Sirenko, A. F.: Materials & Design, 50, 2013, p. 606. [doi:10.1016/j.matdes.2013.02.078](https://doi.org/10.1016/j.matdes.2013.02.078)
- [21] Vlach, M., Čížek, J., Smola, B., Melikhova, O., Vlček, M., Kodetová, V., Kudrnová, H., Hruška, P.: Materials Characterization, 129, 2017, p. 1. [doi:10.1016/j.matchar.2017.04.017](https://doi.org/10.1016/j.matchar.2017.04.017)
- [22] Dlubek, G., Krause, R., Brommer, O.: Journal of Materials Science, 21, 1986, p. 853. [doi:10.1007/BF01117364](https://doi.org/10.1007/BF01117364)
- [23] Antonione, C., Marino, F., Riontino, G., Abis, S., Russo, E.: Materials Chemistry and Physics, 20, 1988, p. 13. [doi:10.1016/0254-0584\(88\)90055-7](https://doi.org/10.1016/0254-0584(88)90055-7)
- [24] Kodetová, V., Vlach, M., Smola, B., Kekule, T., Daniš, S., Kudrnová, H., Málek, J.: Acta Physica Polonica A, 134, 2018, p. 631. [doi:10.12693/APhysPolA.134.631](https://doi.org/10.12693/APhysPolA.134.631)
- [25] Liu, S., Li, C., Han, S., Deng, Y., Zhang, X.: Journal of Alloys and Compounds, 625, 2015, p. 34. [doi:10.1016/j.jallcom.2014.10.195](https://doi.org/10.1016/j.jallcom.2014.10.195)
- [26] Liu, M., Čížek, J., Chang, C. S. T., Banhart, J.: Acta Materialia, 91, 2015, p. 355. [doi:10.1016/j.actamat.2015.02.019](https://doi.org/10.1016/j.actamat.2015.02.019)
- [27] Liu, C. H., Lai, Y. X., Chen, J. H., Tao, G. H., Liu, L. M., Ma, P. P., Wu, C. L.: Scripta Materialia, 115, 2016, p. 150. [doi:10.1016/j.scriptamat.2015.12.027](https://doi.org/10.1016/j.scriptamat.2015.12.027)
- [28] Deschamps, A., Livet, F., Bréchet, Y.: Acta Materialia, 47, 1998, p. 281. [doi:10.1016/S1359-6454\(98\)00293-6](https://doi.org/10.1016/S1359-6454(98)00293-6)
- [29] Buha, J., Lumley, R. N., Crosky, A. G.: Materials Science and Engineering: A, 492, 2008, p. 1. [doi:10.1016/j.msea.2008.02.039](https://doi.org/10.1016/j.msea.2008.02.039)
- [30] Myhr, O. R., Grong, Ø., Andersen, S. J.: Acta Materialia, 49, 2001, p. 65. [doi:10.1016/S1359-6454\(00\)00301-3](https://doi.org/10.1016/S1359-6454(00)00301-3)
- [31] Myhr, O. R., Grong, Ø., Schäfer, C.: Metallurgical and Materials Transactions A, 46, 2015, p. 6018. [doi:10.1007/s11661-015-3175-y](https://doi.org/10.1007/s11661-015-3175-y)
- [32] Starink, M. J.: Thermochemica Acta, 404, 2004, p. 163. [doi:10.1016/S0040-6031\(03\)00144-8](https://doi.org/10.1016/S0040-6031(03)00144-8)
- [33] Afify, N., Gaber, A. F., Abbady, G.: Materials Sciences and Applications, 2, 2011, p. 427. [doi:10.4236/msa.2011.25056](https://doi.org/10.4236/msa.2011.25056)
- [34] Abis, S., Riontino, G.: Materials Letters, 5, 1987, p. 442. [doi:10.1016/0167-577X\(87\)90060-7](https://doi.org/10.1016/0167-577X(87)90060-7)